7.2 INTERMITTENT TURBULENCE IN STRATIFIED FLOW OVER A CANOPY

Steven J. BÖING *, Harm J.J. JONKER
Multi-Scale Physics, Delft University of Technology, The Netherlands
Bas J.H. VAN DE WIEL
Turbulence and Vortex Dynamics, Eindhoven University of Technology, The Netherlands
Arnold F. MOENE
Meteorology and Air Quality, Wageningen University, The Netherlands

ABSTRACT

During the night turbulence can often be very intermittent, occurring in sudden vigorous bursts after prolonged periods of low-intensity. Several mechanisms have been proposed to explain intermittency. The present study focuses on the role of porous surface elements, which influence the mean wind profile near the surface and therefore the shear characteristics. The shape of this profile plays a vital role in the mechanism that causes the flow to destabilize.

Direct numerical simulations of a pressure driven stably stratified flow are used to study the development of initial instabilities into breaking waves and the possibility of a subsequent collapse of turbulence and return to a weakly turbulent state. To better understand the parameter space associated with the occurrence of intermittency, we conduct a linear stability analysis which provides critical values for the Richardson number in relation to the canopy characteristics. This enables one to make an a-priori educated guess of the conditions that favor intermittency, which are subsequently studied in more detail using the DNS.

1. INTRODUCTION

The behavior of the Stable Boundary Layer (SBL) can be broadly classified into 3 different regimes. In the radiative regime, turbulence is almost completely suppressed by buoyancy. The temperature of the atmosphere is determined by the exchange of longwave radiation with the surface. When there is sufficient wind shear, on the other hand, the boundary layer will remain turbulent in spite of stable stratification.

A third type of behavior occurs when episodes of strong and extremely weak turbulence flow alternate. This intermittent behavior is quite common: during the CASES-99 (Cooperative Atmosphere-Surface Exchange Study) field experiment, for example, it occurred during 40 % of nights (Van de Wiel, 2002). The idea that the surface layer may play a role in driving intermittency dates back to the work work Blackader (1957) and Businger (1973). They describe a local mechanism: when turbulence is suppressed due to stratification, the mean wind velocity above the surface can increase rapidly. However, as the shear becomes higher, the gradient Richardson number decreases, and the flow becomes dynamically unstable. A burst of turbulence occurs, energy is extracted from the mean flow, shear decreases and stratification eventually overcomes turbulence. The collapse of turbulence resulting from surface cooling has been studied in a one-dimensional model by Derbyshire (1999) and Van de Wiel et al. (2007). Further studies showed that intermittency can occur due to interaction between the ground surface and the lower boundary layer. In the work of Van de Wiel et al. (2002a and 2002b) and De Ronde et al. (2008), the effect of a vegetation layer that responds rapidly to temperature changes in the atmosphere was of crucial importance.

In the present work, the possible role of canopy waves in intermittency is investigated. The presence of a canopy can strongly contribute to the generation of turbulence in a stratified flow as the porous canopy layer can create an inflection point in the mean wind profile. The turbulence characteristics of the flow at the inflection point above a canopy are similar to that of a mixing layer (e.g. Raupach et al. 1996). The influence of a canopy in a stably stratified flow has been observed by Shaw et al. (1988) and Lee et al. (1997). The latter study found waves persisting over 10 to 80 cycles, a time scale which was related to the persistence of wind shear above the canopy layer.

Previous numerical simulations also looked into the role of the canopy. The stability of an inviscid, stratified flow over a canopy was studied by Lee (1997). A two-dimensional simulation of stratified flow over a canopy was performed by Hu et al. (2002), who found that wave saturation occurred.

Direct Numerical Simulation has been applied before to investigate the collapse of turbulence in a pressure driven boundary layer under stratification by Nieuwstadt (2005). Dörnbrack et al. (1995) used a DNS and an LES to study the behavior of breaking gravity waves resulting from topography in the SBL. The DNS results showed breaking gravity waves at the same critical level as the LES. This problem is in many ways similar to the phenomenon that is investigated here: canopies in a stable atmosphere also generate waves at a critical level. The breaking waves make it possible for turbulence to exist even at low Reynolds numbers, and thus make the problem suitable for DNS.

* *Corresponding author address:* Steef Böing, Dept. of Multi-Scale Physics, Delft University of Technology, Delft, The Netherlands (s.j.boing@tudelft.nl - www.msp.tudelft.nl)

2. METHOD AND CASE

2.1 *System of equations*

We start from the Boussinesq equations for incompressible flow. The flow is driven by a large scale pressure gradient $-\delta_{i1}\partial_x P$. Following Shaw and Schumann (1992), a quadratic drag term is introduced in the momentum equation:

$$\begin{aligned}\partial_t u_i =& - u_j\partial_j u_i + \frac{g}{T_0}\theta\delta_{i3} - \delta_{i1}\partial_x P - \partial_i p + \\ & \nu\partial_{jj}u_i - C_d a(z) u_i (u_j u_j)^{1/2}, \qquad (1a)\\ \partial_t\theta =& - u_j\partial_j\theta + \kappa\partial_{jj}\theta, \qquad (1b)\\ \partial_i u_i =& 0. \qquad (1c)\end{aligned}$$

Here, C_d is a drag coefficient and $a(z)$ the foliage density. We chose a foliage density that varies as a hyperbolic tangent:

$$a(z) = a_{max}\left(\tfrac{1}{2} - \tfrac{1}{2}\tanh\left(\frac{z-h_{can}}{\delta}\right)\right) \qquad (2)$$

The top and bottom of the domain are kept at constant temperatures, and at the top a free-slip boundary condition is implemented. We introduce the following scales for velocity, length, time, temperature and pressure:

$$\begin{aligned}U_{sc} &= \left(-H\frac{dP}{dx}\right)^{1/2},\\ t_{sc} &= H/U_{sc},\\ T_{sc} &= T_{top} - T_{bottom},\\ P_{sc} &= U_{sc}^2.\end{aligned}$$

This allows us to write a non-dimensional system of equations

$$\begin{aligned}\partial_t u_i =& - u_j\partial_j u_i + \mathrm{Ri}\theta\delta_{i3} + \delta_{i1} - \partial_i p + \\ & \frac{1}{\mathrm{Re}}\partial_{jj}u_i - \mathrm{Dr}\alpha(z) u_i (u_j u_j)^{1/2}, \qquad (4a)\\ \partial_t\theta =& - u_j\partial_j\theta + \frac{1}{\mathrm{PrRe}}\partial_{jj}\theta, \qquad (4b)\\ \partial_i u_i =& 0. \qquad (4c)\end{aligned}$$

Here, $\mathrm{Pr} = \nu/\kappa$ is the Prandtl number, $\mathrm{Ri} = gT_{sc}H/T_0U_{sc}^2$ the scaling Richardson number, $\mathrm{Re} = U_{sc}H/\nu$ the scaling Reynolds number and $\mathrm{Dr} = C_d a_{max} H$ the Drag number. Note that the scaling Reynolds number is not based on the maximum flow velocity. For example, the critical Reynolds number at which flow becomes turbulent in plane channel flow is $7\!5.97$ (with the length scale chosen as half the domain height to account for the no-slip boundary condition at the top). Two further scales appear in the expression for the foliage density $\alpha(z) = a(z)/a_{max}$: $\Delta = \delta/H$ is the non-dimensional canopy transition height and $\mathrm{H_{can}} = h_{can}/H$ the non-dimensional canopy height.

2.2 *Stability analysis*

To predict the onset of instabilities, we write the equations of motion in terms of a mean flow, which will be marked with an overbar, and perturbations, denoted by primes. We consider perturbations in the x,z-plane only. The linearized evolution equations for the perturbations read:

$$\begin{aligned}\partial_t u' =& - \overline{u}\partial_x u' - w'\partial_z\overline{u} - \partial_x p' + \frac{1}{\mathrm{Re}}\left[\partial_{xx}+\partial_{zz}\right]u' - \\ & 2\mathrm{Dr}\overline{u}u', \qquad (5a)\\ \partial_t w' =& - \overline{u}\partial_x w' + \mathrm{Ri}\theta' - \partial_z p' + \frac{1}{\mathrm{Re}}\left[\partial_{xx}+\partial_{zz}\right]w' - \\ & \mathrm{Dr}\overline{u}w', \qquad (5b)\\ \partial_t\theta' =& - \overline{u}\partial_x\theta' - w'\partial_z\overline{\theta} + \frac{1}{\mathrm{PrRe}}\left[\partial_{xx}+\partial_{zz}\right]\theta', \qquad (5c)\\ & \partial_x u' + \partial_z w' = 0. \qquad (5d)\end{aligned}$$

The mean flow is taken as a laminar flow, which is allowed to evolve in time. The initial temperature profile is linear, and we start with no mean velocity. For the calculation of critical Reynolds numbers, a fully developed laminar flow is considered. The perturbation analysis is similar to that in Lee (1997), with the differences that viscosity and thermal diffusion are taken into account and that there is a prefactor 2 occurring in the horizontal drag term. An expansion is made in Fourier eigenmodes:

$$\begin{aligned}u'_k(x,z,t) =& \partial_z\psi(z)\, e^{ikx - ikc_R t + kc_I t},\\ w'_k(x,z,t) =& - ik\psi(z)\, e^{ikx - ikc_R t + kc_I t},\\ \theta'_k(x,z,t) =& \hat{\theta}(z)\, e^{ikx - ikc_R t + kc_I t}.\end{aligned}$$

Here, ψ is a complex stream function and $\hat{\theta}$ a complex temperature amplitude. $c = c_R + ic_I$ is the complex phase speed of the wave and k is the wavenumber. Positive values of c_I correspond to unstable (growing) waves.

2.3 *Direct Numerical Simulation*

The DNS uses a second-order Adams-Bashforth time scheme and a Poisson pressure solver. More details on the numerics of the code are given in Van Reeuwijk (2007). A uniform grid with 128 grid points in both horizontal directions and 64 in the vertical was used. Since the DNS is forced with the fastest growing perturbations from the stability analysis, the domain length in the x-direction L_x will be chosen as $n\,(2\pi/k_{pref})$, where n is an integer and k_{pref} is the wavenumber of the initially fastest growing wave in the stability analysis. Results for $n = 1$ (no subharmonics of the fastest growing mode) are presented.

3. RESULTS AND DISCUSSION

3.1 *Stability analysis*

The stability analysis allows us to find a minimum scaling Reynolds number for which instabilities are expected to grow. It was decided to take $\mathrm{Pr} = 1$ and study the effects of Dr and Ri on the critical Reynolds number separately from those of $\mathrm{H_{can}}$ and Δ.

Figure 1 shows the dependence of the critical Reynolds number on Dr and Ri when $\mathrm{H_{can}} = 0.3$ and $\Delta = 0.06$. The critical Reynolds number increases with

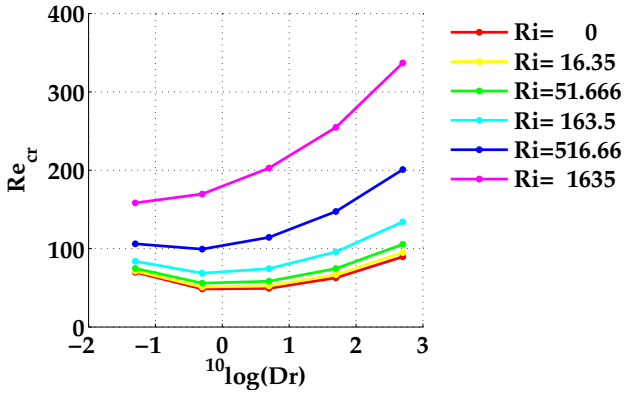

FIG. 1: Critical Reynolds number dependence on Dr and Ri.

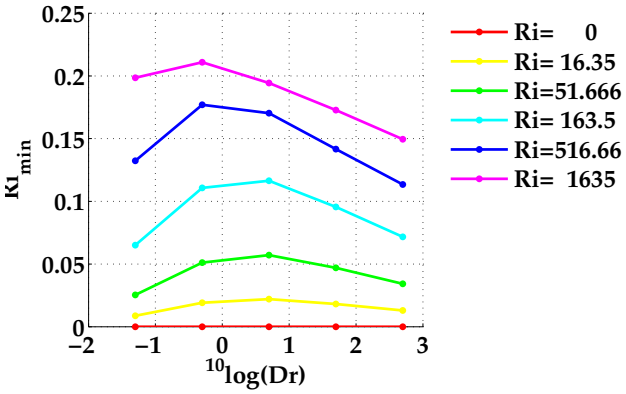

FIG. 2: Diagnosed minimum gradient Richardson number as function of Dr and Ri.

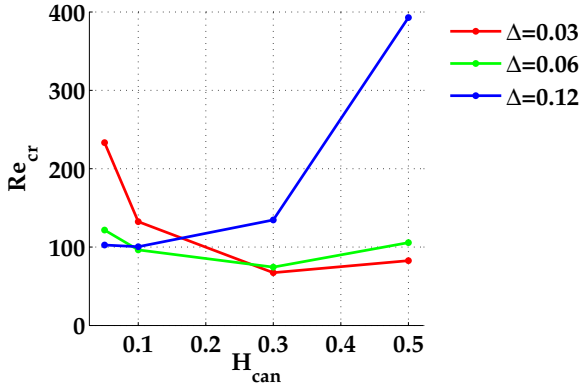

FIG. 3: Critical Reynolds number dependence on $\mathrm{H_{can}}$ and Δ.

the scaling Richardson number, as turbulence is suppressed further at higher stability. As for the influence of the drag number, there is an optimum that corresponds

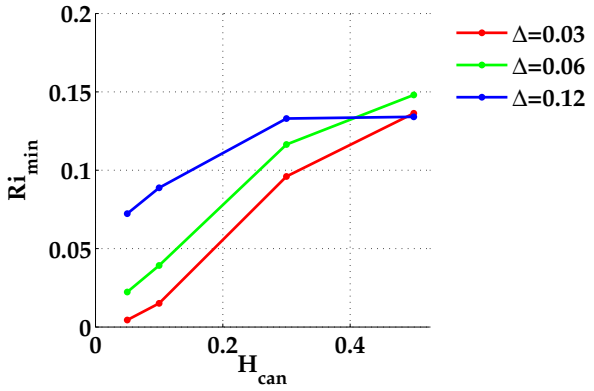

FIG. 4: Minimum gradient Richardson number as a function of $\mathrm{H_{can}}$ and Δ.

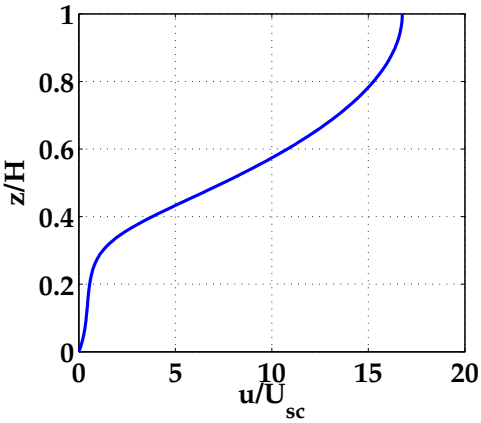

FIG. 5: Along channel velocity profile for the critically unstable case in section 3.1.

to the lowest critical Reynolds number. For a higher drag, motions below the canopy are suppressed to such an extent that it hinders the formation of canopy waves. When the drag approaches either 0 or takes a very large value, the problem reduces to a plane half-channel flow (in the latter case, no flow is possible below the canopy transition), and the inflection point no longer occurs.

Miles and Howard (1964) showed that in stratified, inviscid laminar shear flow, the gradient Richardson number has to be below $1/4$ somewhere in the flow before instabilities can occur. The gradient Richardson number is defined as

$$Ri_g = \frac{(g/T_0)\partial_z \overline{\theta}}{(\partial_z \overline{u})^2 + (\partial_z \overline{v})^2}. \tag{6}$$

The minimum value of the gradient Richardson number, which we will denote by Ri_{min}, is used to see whether the instabilities can be described by Miles' cri-

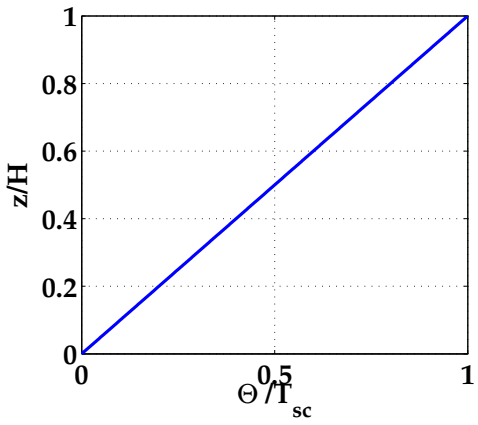

FIG. 6: Along channel temperature profile the critically unstable case.

terion for inviscid stratified shear flow. It is below $1/4$ in all cases, which suggests that drag and viscosity play a significant role (figure 2). For very stable situations, it approaches $1/4$ though.

The influence of $\mathrm{H_{can}}$ and Δ was investigated for $\mathrm{Ri} = 163.5$ and $\mathrm{Dr} = 5$ (figures 3 and 4). It appears that even for a low canopy instabilities occur. The minimum gradient Richardson number is larger when a significant part of the domain is taken up by the canopy. The influence of the transition height Δ depends on the the canopy height, but is relatively small when $\mathrm{H_{can}} = 0.3$ and Δ varies around 0.06.

The characteristics of the case with $\mathrm{Ri} = 163.5$, $\mathrm{Dr} = 5$, $\mathrm{H_{can}} = 0.3$ and $\Delta = 0.06$ are discussed in more detail below. We look at the behavior at the critical Reynolds number of 74.4. The mean horizontal velocity and temperature profiles are shown in figures 5 and 6. The horizontal velocity profile resembles a laminar half-channel flow (parabolic profile) above the canopy. Just above canopy height, a strong curvature of the horizontal velocity profile is found. Below, the wind speed is largely influenced by the presence of the canopy, although the wind shear increases again close to the surface. Since the temperature profile does not have a second derivative, the mean temperature profile does not evolve over time as long as the flow is laminar.

From the eigenmodes, physical quantities such as velocity and temperature perturbations and the kinetic energy of perturbations

$$\mathcal{E} = \tfrac{1}{2}\overline{u'^2 + v'^2 + w'^2}$$

can be calculated (figures 7 and 8). Since the perturbations have a very small amplitude, they are normalized by their maximum values. The normalized perturbation kinetic energy plot also shows the direction of the perturbation velocity field. The fluctuations have the largest amplitude in a shallow layer above the canopy, although a second maximum can also be observed in the lower canopy. The temperature and horizontal velocity have opposite phase below and far above the canopy, in agreement with Lee (1997). It turns out that for the reference case, instabilities do not occur until the minumim gradient Richardson number reaches a minimum value of 0.115 (Fig. 9). Lee also finds gradient Richardson numbers below $1/4$ in his stability analysis.

Miles' criterion for stratified shear flow can be interpreted in terms of the well-posedness of the hydrodynamic equations at a critical level. The growing mode will have a phase speed equal to the mean wind speed at the critical level (Howard, 1961). The occurrence of a strong peak in $\mathcal{E}$ indicates that the occurrence of instabilities in the reference case may also be determined by the behavior of the flow at a critical level. Figure 10 shows the level where $u = c$, which is also where $\mathcal{E}$ peaks. The minimal gradient Richardson number is located slightly below this level. The second derivative of the rescaled velocity is plotted in figure 11. This shows the occurrence of two inflection points which roughly correspond to $\mathcal{E}$ maxima. This all points to the importance of a critical level.

3.2 *Growth rate of perturbations in the DNS*

The case that was discussed in the previous section is also the basis for the DNS simulations. However, in these simulations, a higher Reynolds number is used in order to be able to study intermittency. The results that are presented below use $\mathrm{Re} = 316.2$.

As a test of the consistency between DNS and stability analysis, we considered the growth rate of disturbances. As an initial condition, a steady state for laminar flow is determined by integrating the laminar flow over a large number of time steps in a one dimensional model. The corresponding temperature and velocity profiles are dynamically unstable. A stability analysis of these profiles gives a prediction of the growth rate. The advantage of using a fully developed profile, instead of a developing laminar profile starting from rest, is that the mean flow does not change during the initial growth of small perturbations. The growth rate of perturbations in the DNS should be constant and correspond almost exactly to the growth rate predicted by the stability analysis.

The effect of random perturbation on the fully developed flow was investigated first. The nondimensional time step used was $\triangle t = 7.906 \cdot 10^{-5} t_{sc}$, the temperature perturbations had an amplitude of $A_{pert} = 2 \cdot 10^{-7} T_{sc}$ and the predicted growth rate optimal perturbations was $\sigma_{I,opt} = 14.03 t_{sc}^{-1}$. Figure 12 shows the development of domain integrated velocity and temperature variances and $\mathcal{E}$ in a logarithmic plot. It can be seen that after $t = 0.3$, the temperature disturbances start growing almost linearly. An evaluation of σ_I between $t = 0.76 t_{sc}$ en $t = 0.95 t_{sc}$ gives $13.87 t_{sc}^{-1}$, which is close to the result from the stability analysis. Figures 13 and 14 show the same case, but now forced with optimal perturbations from the stability analysis. Linear growth is found from the beginning. σ_I between $t = 0.76 t_{sc}$ en $t = 0.95 t_{sc}$ is

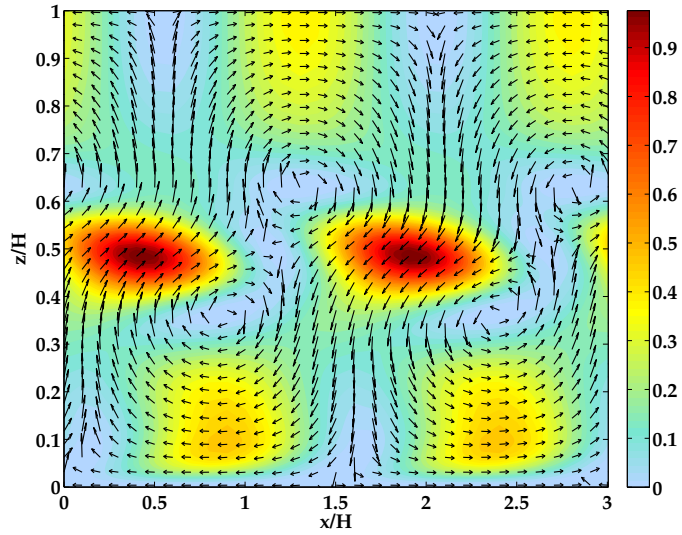

FIG. 7: Perturbation kinetic energy ($\mathcal{E}$) field for the critically unstable case; also the direction (not the magnitude) of the perturbation velocity field is shown.

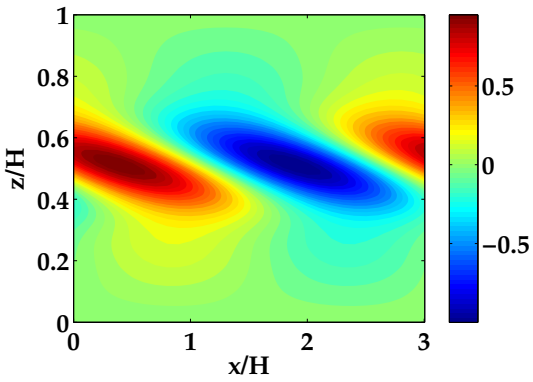

FIG. 8: Temperature perturbations for the critically unstable case.

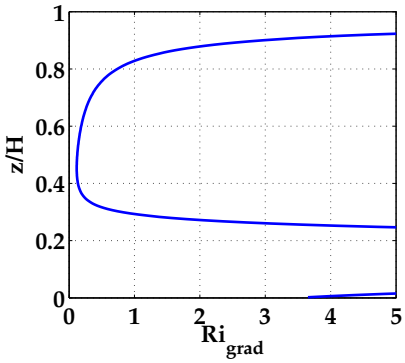

FIG. 9: Gradient Richardson number profile for the critically unstable case .

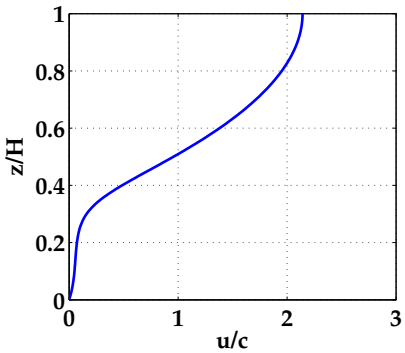

FIG. 10: Velocity profile scaled with the phase speed of the fastest growing mode for the critically unstable case.

$13.99t_{sc}^{-1}$, which corresponds even better to the stability analysis.

3.3 *DNS of intermittent turbulence*

In order to investigate intermittency, we use a simulation with the same settings, but developing from a rest state. To save DNS computing time, a one-dimensional model of the developing laminar flow is coupled to the stability analysis in order to find an initial condition where perturbations have just started to develop. Velocity and temperature fluctuations corresponding to the most unstable eigenmode are introduced in the first time step. The behavior of the perturbations during the first time-steps is shown in figure 15. The perturbation starts growing very slowly. An increase in the growth rate can be observed (at the beginning the growth rate should be close to zero,

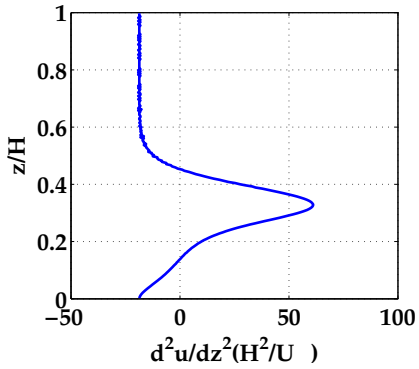

FIG. 11: Rescaled second derivative of the mean velocity profile, indicating two inflection points, for the critically unstable case .

as it has just become unstable).

Figure 16 shows the development of the mean velocity at $z = H$ and $z = H/2$, the domain averaged variances $\overline{u'^2}$, $\overline{v'^2}$, $\overline{w'^2}$, and the sum of these variances $2\mathcal{E}$. The plot of $2\mathcal{E}$ shows overshooting and saturation behavior. Saturated waves have also been found in the earlier studies by Dörnbrack et al. (1995) and Hu et al. (2002). Note that the mean horizontal velocity has not yet reached an equilibrium value at the end of this run. The variance of the spanwise velocities remains 0. In this direction, there is no source of heterogeneity.

However, when a small additional random forcing is applied to the initial temperature field, three-dimensional structures have the opportunity to develop, as shown in figure 17. At $t = 9t_{sc}$, the initial two-dimensional instability has grown to a significant size. At this point, the variance of the spanwise flow $\overline{v'^2}$ is still negligible. After another $3t_{sc}$, suddenly a large three-dimensional instability develops. Three-dimensional instabilities apparently start growing when the two-dimensional wave has already developed.

Once the turbulence has developed, the mean flow start to decelerate. Around $20t_{sc}$, there is an increase in the mean velocity above the canopy, followed by an increase in turbulence. After $35t_{sc}$, however, the turbulence completely disappears and the flow starts accelerating again, until another burst of turbulence occurs. This behavior continues over several cycles. The later bursts are not preceded by two-dimensional waves.

The velocity and temperature profiles before and after a number of turbulent episodes are shown in figures 18 and 19. For the 2 later events, the velocity and temperature profiles are almost the same, both before and after the burst. This suggests that the bursting events are well-defined, even though the turbulence intensity in between bursts fluctuates. The temperature profile is strongly mixed by turbulence.

4. CONCLUSIONS

The aim of the current work was to create a relatively simple framework to study intermittency induced by a porous canopy in a fundamental way. The model that was developed allows for a stability analysis that predicts the transition from laminar to turbulent flow, and can also be used for direct numerical simulation.

Instabilities are found for a wide range of parameter settings, and even at relatively low Reynolds numbers (Re of less than 100). When the perturbations are applied in the DNS, two-dimensional wave growth can be studied in detail. The perturbations eventually saturate, but three-dimensional turbulence results when small random temperature disturbances are added. It was shown that the model can display intermittent behavior at a low Reynolds number. The turbulence occurs as a burst, during which the production of fluctuation kinetic energy $\mathcal{E}$ is large.

During the burst, kinetic energy is extracted from the mean flow and the shear stress decreases. Because stratification is enforced, the flow quickly returns to a weakly turbulent state. After a while, turbulence may even collapse completely. However, in the absence of strong turbulence, the mean flow will be accelerated by the pressure gradient. The increasing shear will lead to the generation of turbulence again, completing the intermittent cycle.

The occurrence of a collapse of turbulence in the DNS may depend on the parameter settings of the model and the Reynolds number. Future work should investigate if the same mechanism also applies to higher Reynolds number flow.

ACKNOWLEDGMENTS

This work was sponsored by the National Computing Facilities Foundation (NCF) for the use of supercomputer facilities, with financial support of NWO. The authors like to thank Dr. Han van Dop and Wiet de Ronde for their valuable input during the project.

REFERENCES

Blackader, A., 1957: Boundary-layer wind maxima and their significance for the growth of nocturnal inversions. *Bulletin of the American Meteorological Society*, **38**, 283–290.

Businger, J., 1973: Turbulent transfer in the atmospheric surface layer. *Workshop on the Planetary Boundary layer*, D. Haugen, Ed., Am. Met. Soc., 67–98.

De Ronde, W., H. Jonker, B. Van de Wiel, and A. Moene, 2008: A numerical and analytical study of intermittency in the stable boundary layer. *18th AMS Symposium on Boundary Layers and Turbulence*.

Derbyshire, S., 1999: Boundary-layer decoupling over cold surfaces as a physical boundary instability. *Boundary Layer Meteorol.*, **90**, 297–325.

Dörnbrack, A., T. Gerz, and U. Schumann, 1995: Turbulent breaking of overturning gravity waves below a critical level. *Applied Scientific Research*, **54**, 163–176.

Howard, L., 1961: Note on a paper of John W. Miles. *J. Fluid. Mech.*, **10**, 509–512.

Hu, X., X. Lee, D. Stevens, and R. Smith, 2002: A numerical study of nocturnal wavelike motion in forests. *Boundary Layer Meteorol.*, **102**, 199–223.

Lee, X., 1997: Gravity waves in a forest: A linear analysis. *J.Atmos.Sci.*, **54**, 2574–2585.

Lee, X., H. Neumann, G. den Hartog, J. Fuentes, T. Black, R. Mickle, P. Yang, and P. Blanken, 1997: Observation of gravity waves in a boreal forest. *Boundary Layer Meteorol.*, **84**, 383–398.

Miles, J. and L. Howard, 1964: Note on a heterogeneous shear flow. *J. Fluid. Mech.*, 331–336.

Nieuwstadt, F., 2005: Direct numerical simulation of stable channel flow at large stability. *Boundary Layer Meteorol.*, **116**, 277–299.

Raupach, M., J. Finnigan, and Y. Brunet, 1996: Coherent eddies and turbulence in vergetation canopies: the mixing-layer analogy. *Boundary Layer Meteorol.*, **78**, 351–382.

Shaw, R., G. den Hartog, and H. Neumann, 1988: Influence of foliar density and thermal stability on profiles of reynolds stress and turbulence intensity in a deciduous forest. *Boundary Layer Meteorol.*, **45**, 391–409.

Shaw, R. and U. Schumann, 1992: Large-eddy simulation of turbulent flow above and within a forest. *Boundary Layer Meteorol.*, **61**, 47–64.

Van de Wiel, B., 2002: Intermittent turbulence and oscillations in the stable boundary layer over land. Ph.D. thesis, Wageningen University.

Van de Wiel, B., A. Moene, R. Ronda, H. de Bruin, and A. Holtslag, 2002a: Intermittent turbulence and oscillations in the stable boundary layer over land. part ii: A system dynamics approach. *Journal of the Atmospheric Sciences*, **59**, 2567–2581.

Van de Wiel, B., A. Moene, G. Steeneveld, O. Hartogensis, and A. Holtslag, 2007: Predicting the collapse of turbulence in stably stratified boundary layers. *Flow Turbulence Combustion*, **79**, 251–274.

Van de Wiel, B., R. Ronda, A. Moene, H. de Bruin, and A. Holtslag, 2002b: Intermittent turbulence and oscillations in the stable boundary layer over land, part i: A bulk model. *Journal of the Atmospheric Sciences*, **59**, 942–958.

Van Reeuwijk, M., 2007: Direct simulation and regularization modelling of turbulent thermal convection. Ph.D. thesis, Delft University of Technology.

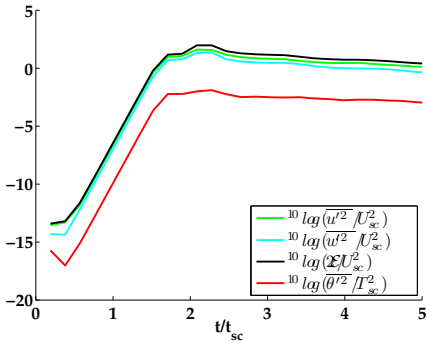

FIG. 12: Growth of perturbations, with a laminar steady state profile and random temperature perturbations

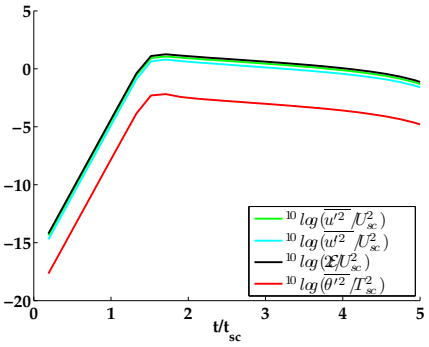

FIG. 13: Growth of perturbations, with a laminar steady state profile and optimal perturbations

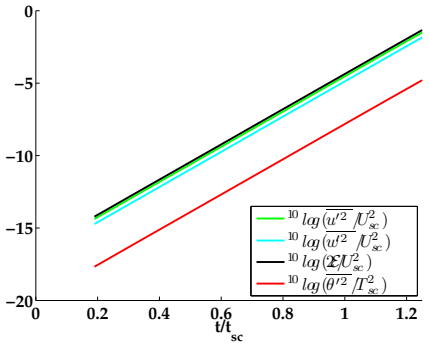

FIG. 14: As previous figure, but only the first few time steps

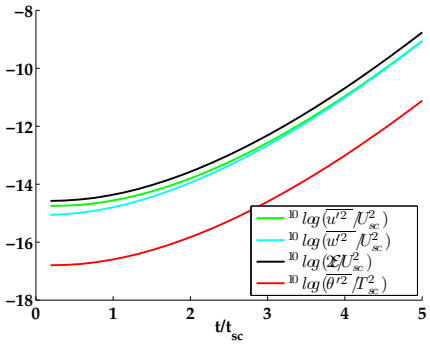

FIG. 15: Growth of perturbations, with a developing profile and optimal perturbations

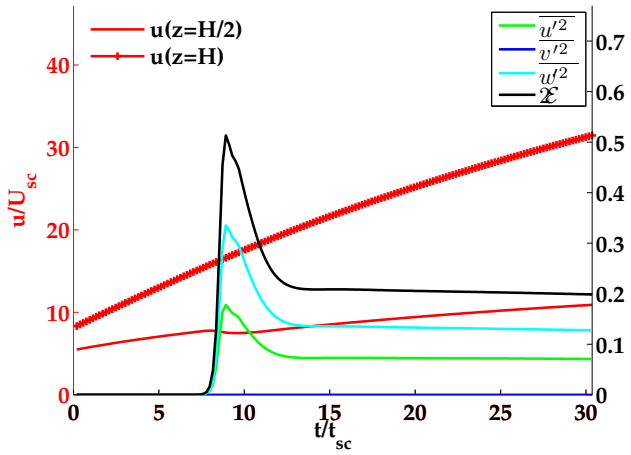

FIG. 16: Mean streamwise velocity at 2 levels and domain integrated $2\mathcal{E}$, with optimal perturbations only

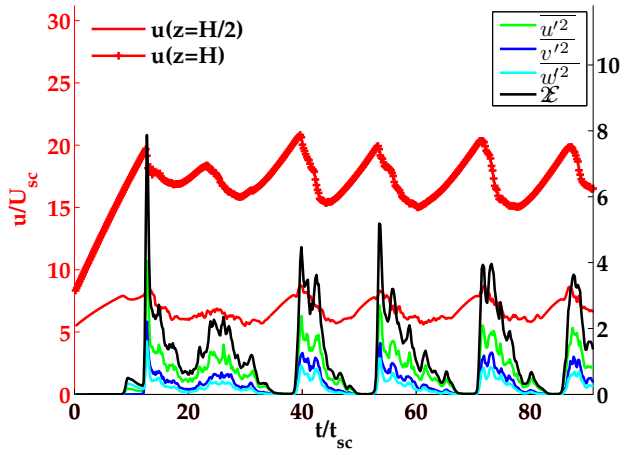

FIG. 17: Mean streamwise velocity at 2 levels and domain integrated $2\mathcal{E}$, with added initial random temperature perturbations

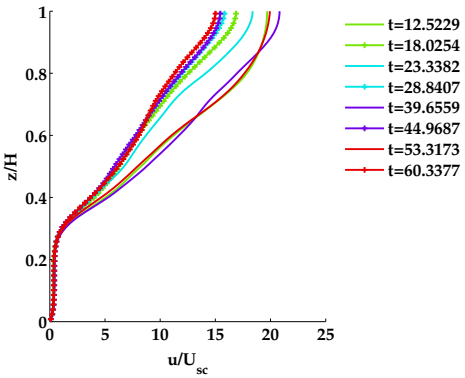

FIG. 18: Velocity profiles before (solid lines) and after (with markers) a number of bursting events

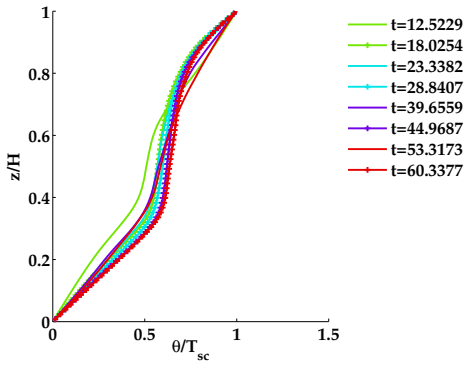

FIG. 19: Temperature profiles before (solid lines) and after (with markers) a number of bursting events